PHYSICAL REVIEW B VOLUME 32, NUMBER 11 1 DECEMBER 1985

Magnetic behavior of free-iron and iron oxide clusters

D. M. Cox, D. J. Trevor, R. L. Whetten,* E. A. Rohlfing,† and A. Kaldor
Corporate Research, Exxon Research and Engineering Company, Route 22 East, Annandale, New Jersey 08801
(Received 22 February 1985; revised manuscript received 18 July 1985)

We report the first measurement of the magnetic properties of isolated iron-atom clusters ranging in size from 2 to 17 atoms as well as the magnetic behavior of the monoxides and dioxides of (2—7)-atom iron clusters. Production of metal clusters is initiated by laser vaporization of an iron rod inside the throat of a high-pressure pulsed nozzle. The neutral metal cluster beam passes through a Stern-Gerlach magnet and the deflected beam is detected by spatially resolved time-of-flight photoionization mass spectrometry. From our analysis we conclude that the spin per atom of iron clusters is at least that of bulk iron, suggesting these small clusters are the precursors to bulk ferromagnetic iron.

I. INTRODUCTION

The measurement of the fundamental properties of small clusters are of great interest in increasing our understanding of the nature of the chemical bond and as benchmarks for theoretical approaches. Just recently it has become possible to study dimers, trimers, and larger clusters in an environment free from the perturbing influence of inert gas matrices, but still at sufficiently low temperature that spectroscopic measurements are not overly complicated by thermal excitation. With use of pulsed cluster beam sources, new experimental investigations of the optical spectroscopy of a variety of metal dimers[1,2] have provided fundamental answers regarding bonding character and bond length of several metal dimers. These and other investigations of small metal clusters have been instrumental in instigating renewed theoretical investigations with the aim of quantitative predictions of the properties of these few-atom systems. Obviously, as many-electron systems they are far from simple, theoretically or experimentally.

Historically,[3] following Stern and Gerlach's original landmark experiment with silver atoms, nonresonant magnetic deflection experiments were performed on many atomic systems. However, in that era only effusive sources were available, with a resulting velocity distribution which made unambiguous interpretation of the deflection patterns very difficult except for the simplest atomic and molecular species. Thus the straightforward measurements of magnetic deflection patterns upon passage of a neutral atomic or molecular species through a single inhomogeneous magnetic field rapidly gave way to magnetic resonance methods which in simplest form required three magnetic fields. The first field was an inhomogeneous field used for velocity and state selection, followed by a homogeneous field region for inducing state changes, and finally a second inhomogeneous field for refocusing the particular velocity and state selected species on the detector.[3] The difficulty of producing an intense beam of metal clusters and the broad velocity distribution of effusive sources effectively account for the fact that, except for one report[4] on potassium clusters, experimental information on the magnetic properties of isolated metal clusters is nonexistent. With the development of pulsed laser vaporization of metal substrates inside a high-pressure pulsed nozzle, synthesis of new materials,[1,2,5] i.e., clusters of two to hundreds of atoms, is now a reality. The combination of this synthetic technique with pulsed laser photoionization and time-of-flight mass spectrometry, which is both velocity and mass selective, makes it feasible to perform simple magnetic deflection experiments on clusters of almost any material.

In this paper we report the first experiments on the magnetic behavior of free-iron and iron-oxide clusters by examining the Stern-Gerlach deflection pattern of individual mass-selected clusters. We find that iron clusters composed of two to 17 atoms are paramagnetic, possessing magnetic moments which increase linearly with cluster size. These results on iron clusters are compared with theoretical predictions of the magnetic nature of certain iron clusters[6—8] and with measurements on bulk iron.[9]

II. EXPERIMENTAL SECTION

A. Cluster beam production and deflection

The metal cluster source, molecular-beam apparatus, and photoionization time-of-flight mass spectrometer (TOFMS) have been described in detail elsewhere.[5,7] To briefly summarize, the cluster beam source is a high-pressure, pulsed nozzle with added faceplates and extender channels through which a carrier gas (helium or neon) at a backing pressure near 10 atm expands into vacuum. The faceplate holds a continuously rotating and translating metal target rod from which metal vapor, produced via pulsed-laser vaporization, is entrained in the helium or neon flow. Cluster formation occurs in the channel and is rapidly quenched when the gas flow expands into vacuum. This free-jet expansion also cools the random translational, rotational and, to a lesser extent, vibrational motions of the clusters. The expansion is collimated by one or more skimmer cones and then crossed by a probe laser beam which produces photoions to be analyzed by the TOFMS. The TOFMS signal is digitized,

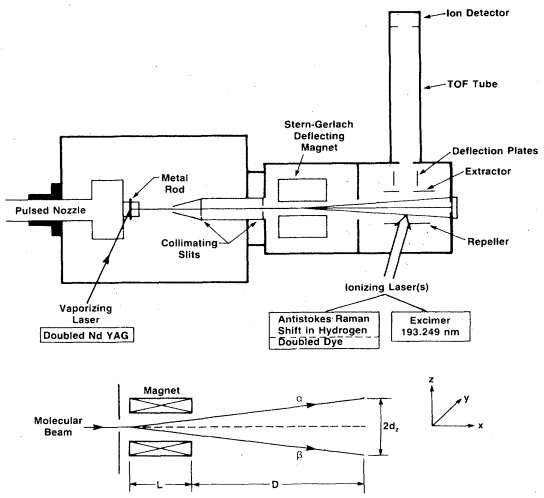

FIG. 1. Schematic of the pulsed molecular-beam apparatus and schematic of the geometrical arrangement for magnetic deflection of the metal-atom clusters.

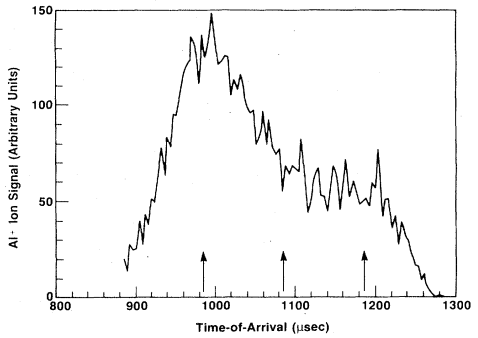

FIG. 2. Aluminum-atom ion signal is plotted as a function of delay time between firing the vaporizing laser pulse and the ionizing laser pulse. Neon carrier gas was used for this time-of-arrival spectrum.

stored on a Digital Equipment Corporation (LSI 11/23) computer system, and converted to a cluster mass spectrum.

For the experiments described in this paper, shown schematically in Fig. 1, a Stern-Gerlach magnet with cylindrical Rabi pole tips is installed on the beam axis 58 cm downstream from the metal vaporization region. Two collimating slits, one mounted on the magnet entrance and the other 26 cm upstream from the magnet and 32 cm downstream from the vaporization region, serve to define a narrow (0.025 by 0.3 cm) rectangular slice of the cluster beam which enters the magnet at the center of the pole gap space. At the photoionization region the cluster beam is scanned by translating the cylindrically focused [0.04 cm high full width at half maximum (FWHM) by 1 cm long] ionizing laser beam vertically across the molecular beam. The width of the cluster beam at the ionizing region is found to be $\sim$0.06 cm (FWHM), consistent with the size expected from geometrical consideration of the collimating slit widths and positions.

B. Velocity selection

To obtain a TOF mass spectrum, the ionizing laser beam (ArF, 10 ns pulse width) is fired at a fixed delay relative to the vaporizing laser. By varying the delay time between the vaporizing laser beam and the ionizing laser beam, the neutral cluster beam TOF distribution can be measured. The pulsed-laser ionization also performs a velocity selection of the clusters, eliminating the velocity distribution effects which occur with effusive beams. A TOF spectrum for the Al atom with neon carrier gas is shown in Fig. 2. All clusters exhibit a similar TOF spectrum, demonstrating that they all have a nearly identical velocity distribution peaked at a velocity independent of cluster size.

The magnetic properties of clusters are examined in two ways. The spatial deflection patterns are measured by spatially translating the ionizing laser beam across the molecular beam at a fixed magnetic field strength. Alternatively, the ionizing laser is set at a fixed position relative to the molecular beam, and the field strength is varied to deflect individual magnetic substates through the detection region. Throughout this paper we will refer to the first of these as spatial scans and the second as field scans.

Referring to the coordinate system shown in Fig. 1, the deflection in the z direction of a species, i, with a magnetic moment μ_i, and masses m_i, is given as

$$d_i=\mu_i\frac{\partial H}{\partial z}L^2\frac{1+2D/L}{2m_i v_{xi}^2}\ , \tag{1}$$

where L is the length of the magnet, $\partial H/\partial z$ is the gradient of the magnetic field, D is the distance from the end of the magnet to the detection region, and v_{xi} is the velocity of the species through the magnet, whose axis is aligned parallel to the x axis. Since D and L are known from the physical characteristics of the apparatus, and the deflection d_i and mass m_i are experimentally measured quantities, the measurement of a cluster with a known moment μ allows us to obtain the ratio of the gradient to the square of the velocity $(\partial H/\partial z)/v^2$.

C. Calibration

Unknown moments, μ_x, can be obtained by referencing to a known moment such as that of the iron or aluminum atom. The magnetic moment of the iron or aluminum atom is easily calculable from the parameters listed in Table I using the relation

TABLE I. Properties of Al and Fe atoms.

	Al	Fe
Ground state	$^2P_{1/2}$	$^5D_4$
g factor	$\frac{2}{3}$	$\frac{3}{2}$
M_J values	$\pm\frac{1}{2}$	±4, ±3, ±2, ±1, 0
Mass	27 amu	56 or 54 amu
$\mu=M_J g\mu_0$	$\pm\frac{1}{3}\mu_0$	$\pm6\mu_0$, $\pm4.5\mu_0$, $\pm3\mu_0$, $\pm1.5\mu_0$, 0

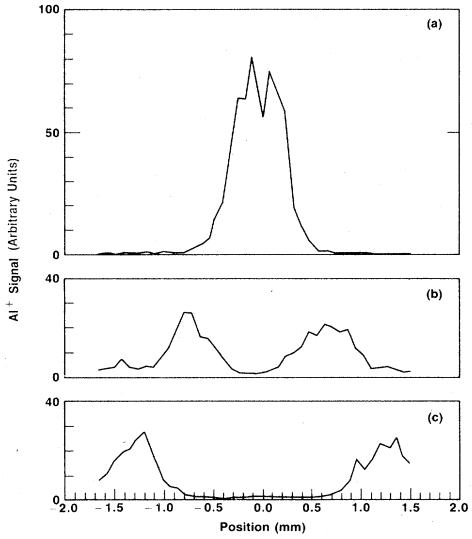

FIG. 3. Spatial scan of aluminum-atom signal as a function of position for (a) $\partial H/\partial z=0$ kG/cm, (b) $\partial H/\partial z=50.8$ kG/cm, (c) $\partial H/\partial z=84.5$ kG/cm.

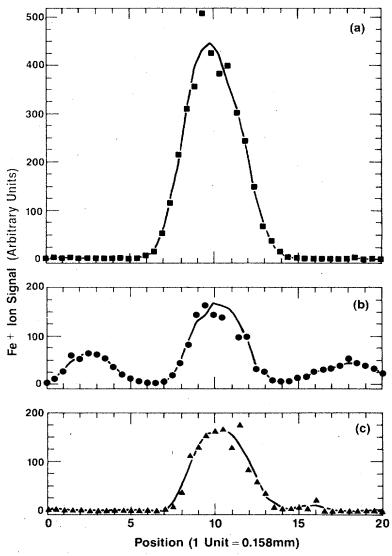

FIG. 4. Spatial scan of the iron atom at (a) 0, (b) 50.8 kG/cm, and (c) 84.5 kG/cm magnetic field gradient using neon carrier gas. The solid line is a seven-point spline smoothing of the data.

$$\mu_J = gM_J\mu_0 , \tag{2}$$

where g is the Landé g factor, μ_0 is the Bohr magneton, and M_J is the z component of the total angular momentum J. Typical spatial scans for the aluminum atom using neon carrier gas are shown in Fig. 3 for three different magnetic field gradients. Similar results for the iron atom are shown in Fig. 4, except that helium was used as the carrier gas. For aluminum with neon carrier gas, complete separation of the two magnetic substates ($\pm\frac{1}{2}\mu_0$) is observed. With helium as the carrier gas complete spatial separation of the two Al magnetic substates is not obtained due to the limited deflecting power of the magnet. The iron atom has a $^5D_4$ ground electronic state and $2J+1=9$ magnetic substates. Figure 4 shows that at a medium field gradient the lowest $M_J=1$, $\mu=1.5\mu_0$ magnetic substate is resolved from the $M_J=0$ substate, and that at an even higher field only the $M_J=0$ substate can be observed. Additionally, we note that the ratio of the deflection measured at different field gradients for the atoms (Al or Fe) is the same as the ratio of the field gradients predicted from previous calibration curves.[10] This implies that the shape of the calibration curve has not changed and suggests that the absolute field values are nearly the same as previously calibrated. Except for the discussion below regarding beam velocity and stagnation temperature, our results do not rely on knowledge of the absolute value for the field gradient or velocity, but only on knowledge of the ratio of gradient to the square of the velocity which is obtained directly from measurements of atom deflection.

In order to estimate the actual beam velocity associated with a particular time of arrival, this beam flight time, defined as the time for the clusters to travel from the end of the extender to the photoionization zone, must be determined. A time-of-arrival spectrum represents the ion signal dependence on total delay time between the firing of the vaporizing laser pulse and the ionizing laser pulse. However, the cluster speed in the extender is slower than in the molecular beam. The beam flight time for the Al atom is estimated from measured deflections at different times of arrival assuming the magnetic field from calibration curves[10] and using Eq. (1) to calculate the beam velocity. Table II summarizes the results: the beam velocity is given in column 4, and the beam flight time is given in column 5.

The 985-μsec total flight time near the center of the profile corresponds to a velocity of 1.5×10^5 cm/sec. The time-of-arrival profile shown in Fig. 2, when transformed to its equivalent velocity distribution, has a velocity spread $\Delta v/v=0.14$, where Δv is the FWHM of the velocity distribution about the average velocity. For supersonic beams the degree of cooling of translational degrees of freedom is given by

$$T\approx T_0(\Delta v/v)^2 , \tag{3}$$

where T_0 is the stagnation temperature of the nozzle.[11] Using the relationship that $T_0=mv^2/5k$ with a velocity of 1.5×10^5 cm/sec a stagnation temperature of 1080 K is back calculated for neon carrier gas results, an appreciable increase over the local ambient nozzle temperature of 300 K. This increase can be rationalized by recognizing that since a significant amount of metal is being evaporated from the surface of a metal rod, the local heating must be in excess of 1030 K, the melting point of aluminum. For clusters to grow and be stabilized during the transit through the extender tube, much of this heat of formation must be transferred to the carrier gas, thereby increasing the stagnation temperature. With the rapid adiabatic expansion from the extender tube into vacuum, the translational, rotational, and vibrational energy will be signifi-

TABLE II. Deflection of aluminum atom at different flight times.

Total flight time (μsec)	Magnetic[a] field gradient (kG/cm)	Measured deflection (mm)	Calc.[b] velocity (cm/sec)	Beam[c] flight time (μsec)
985	79.4	0.91	1.5×10^5	610
985	50.8	0.57	1.5×10^5	610
1085	79.4	0.117	1.36×10^5	673
1185	79.4	0.125	1.28×10^5	715
1185	50.8	0.76	1.31×10^5	700

[a]For the Rabi pole tips, the magnetic field and gradient are closely approximated by that of a two-wire field which can be solved analytically. In these experiments, the magnet is aligned so as to have the undeflected molecular beam pass through the geometrical center of the magnet for which $\partial H/\partial z \approx 5.7H$. From the published calibration curves (Ref. 10) the value of the field, H, as a function of the current through the coils is obtained and thus with the expression above the gradient is obtained.
[b]Velocity is calculated from Eq. (1).
[c]Beam flight time is calculated from S'/v_{beam}, where $S'=91.5$ cm is in the distance from the end of the nozzle extender channel to the photoionization region and v_{beam} is given in the fourth column of the table.

cantly reduced. From the stagnation temperature of 1080 K predicted above and $\Delta v/v$ of 0.14 from the velocity distribution, a translational temperature of $\sim$22 K is estimated.

All measurements which are calibrated with respect to the aluminum or iron atom give the same results within experimental error. We point out that when helium is used as the carrier gas the back-calculated stagnation temperature is about a factor of 2 lower than for neon carrier gas, suggesting that helium is more effective in heat transfer during flow through the extender channel. This is also confirmed by the qualitative observation that larger clusters are produced with helium carrier gas than with neon carrier gas under otherwise identical operating conditions.

III. RESULTS

As stated in the Experimental section two types of measurements were performed: spatial scans of the deflection pattern at fixed magnetic field gradient or magnetic field gradient scans at a fixed deflection position. Figures 3 and 4 are examples of the former and are performed for calibration purposes as discussed in the last section. Spatial scans are much more time consuming and less reproducible than magnetic field scans but are necessary to locate and measure the spatial extent of the cluster beam. Once the cluster beam is located, the ionizing laser beam position is fixed relative to the molecular beam and the magnetic field gradient is varied. Figure 5 depicts the iron-atom ion signal dependence on the magnetic field gradient for three different spatial positions, while Fig. 6 shows a typical magnetic field scan for Fe, Fe_2, Fe_3, and Fe_2O for a fixed displacement of 0.159 cm of the ionizing laser beam below the cluster beam center.

By reference to the iron atom, quantitative values for the moment associated with the highest-spin angular momentum component are obtained. This is done in the following way. The ionizing laser beam is positioned sufficiently far off axis, e.g., at the 0.124-cm position of Fig. 5, so that negligible ion signal is present at zero-field gradient. As the field gradient is increased, the highest moment substate of an individual cluster will be the first to appear as signal. At fixed deflection we see from Eq. (1) that the ratio of the moment of the cluster to that of the atom is simply the product of the ratio of their respective masses times the inverse ratio of their magnetic field gradients, since all other terms in Eq. (1) identically cancel. Thus, at fixed displacement, measurement of the threshold magnetic field gradient for which mass-selected ions just appear allows a lower bound of the cluster magnetic moment to be determined relative to the known moment of the iron atom. From many such scans at varying displacement from the beam axis we have determined a magnetic moment of $(6.5\pm1)\mu_0$ for Fe_2, $(8.1\pm1)\mu_0$ for Fe_3, and $(6.5\pm1)\mu_0$ for Fe_2O.

In addition to these quantitative values for the magnetic moments of Fe_2, Fe_3, and Fe_2O, the qualitative magnetic behavior of the larger Fe_n ($n=4$—17), Fe_nO, and Fe_nO_2 ($N=2$—7) has been examined. We do this by positioning

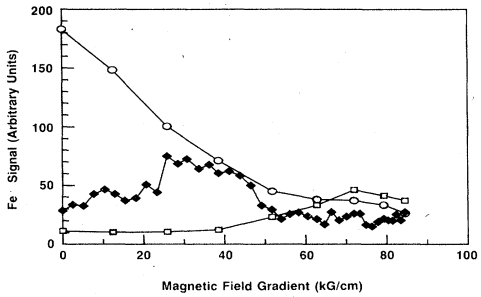

FIG. 5. Dependence of iron-atom ion signal on the magnetic field gradient with the ionizing laser located at different displacements from beam axis with helium as the carrier gas. For the open circles the ionizing laser is positioned on the center molecular-beam axis, for the solid diamonds the ionizing laser is 0.050 cm below the beam axis and for the open squares the ionizing laser is 0.125 cm below the beam axis.

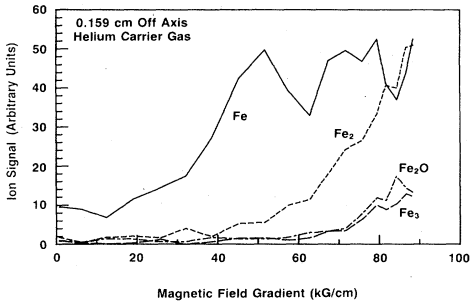

FIG. 6. The dependence of the ion signal for Fe, Fe_2, Fe_3, and Fe_2O as a function of the magnetic field gradient at a displacement of 0.159 cm off axis for the ionizing laser. Helium is the carrier gas.

the ionizing laser beam on-axis and collecting TOF mass spectra as a function of magnetic field gradient. Figure 7 shows two mass spectra, one at zero gradient and one obtained at high magnetic field gradient using neon as the carrier gas. Note that all Fe_n, Fe_nO, and Fe_nO_2 ion signals are substantially reduced at high gradient. Depletion occurs because those magnetic substates which have sufficiently large moments are deflected out of the ionizing zone. The ion signal on clusters other than Fe, Fe_2, and Fe_3 is sufficiently weak that off-axis measurements were not feasible due to poor signal to noise. This is due to the fact that an ion signal for a single magnetic substate will be only $2S+1$ of the total ion signal for a particular cluster with spin S. For high-spin clusters this factor is expected to vary from 7 for the dimer to >40 for Fe_{15}. Thus the maximum off-axis signal would be only $\frac{1}{7}$ to $\frac{1}{40}$ of the initial ion signal for an individual magnetic substate of Fe_2 or Fe_{15}, respectively. Table III presents the measured depletion factors for iron clusters calculated

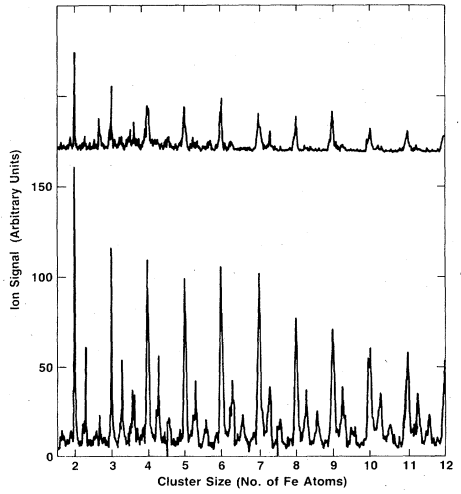

FIG. 7. Time-of-flight mass spectrum for iron clusters at magnetic field gradients of 0 (lower curve) and 84.5 kG/cm (upper curve). The ionizing laser beam is positioned on axis and neon is the carrier gas.

TABLE III. Depletion factors for bare iron clusters.

Cluster	Depletion factor
Fe_2	4.0±0.5
Fe_3	3.3±0.4
Fe_4	3.3±0.7
Fe_5	3.8±0.4
Fe_6	4.3±0.6
Fe_7	4.5±0.6
Fe_8	4.2±0.4
Fe_9	4.8±1.2
Fe_{10}	4.9±0.4
Fe_{11}	5.2±0.4
Fe_{12}	4.5±0.5
Fe_{13}	4.3±0.9
Fe_{14}	4.7±0.8
Fe_{15}	4.8±1.0
Fe_{16}	4.0±0.7
Fe_{17}	3.8±2.4

from the ratio I_0/I_H, where I_0 is the ion signal at zero gradient and I_H is the ion signal at $\partial H/\partial z$ gradient.

The oxide clusters Fe_nO and Fe_nO_2 also interact strongly with the inhomogeneous magnetic field. The depletion factor for Fe_nO clusters $n=3$–7 are (20 to 70%) higher than the corresponding bare Fe_n cluster, while the Fe_nO_2 clusters have depletion factors about the same as the corresponding bare cluster. This implies that the magnetic moments of the oxide clusters will be comparable to or exceed those of the corresponding bare cluster.

IV. DISCUSSION

Anticipating the discussion below, our major experimental results are that all bare and oxided iron clusters are paramagnetic and the magnetic moments of iron clusters increase linearly with increasing number of atoms in the cluster. This statement is supported by the quantitative measurement of the magnetic moment for the dimer, trimer, and dimer oxide and by the on-axis depletion measurements on larger clusters.

In all that follows we assume that the magnetic field ($H_{\max}\sim 15$ kG) is sufficiently high and that the coupling energies of spin angular momentum with rotation and orbital angular momentum are sufficiently weak that spin angular momentum is decoupled from orbital and rotational angular momentum but is strongly coupled to the magnetic field, i.e., the molecular analog of the Paschen-Back effect occurs. The above assumption is justified since the magnetic moment associated with rotation is so small. An orbitally nondegenerate electronic state will always have its resultant spin only weakly coupled to the axis of rotation, and therefore it is easily uncoupled by an external magnetic field.[12(a)] Thus, all multiple states ($S\neq 0$) with zero orbital angular momentum will have a magnetic moment, $\mu_H=2M_S\mu_0$. For species which can have electronic orbital momentum Λ (i.e., diatomics or linear molecules) an additional magnetic moment of $\mu_H=\Lambda^2 M_J\mu_0/J(J+1)$ exists along the field direction.

This term decreases as $1/J$ and thus rapidly becomes negligible compared to the spin moment (assuming $S \neq 0$) for all but the lowest rotational states. In addition, it is likely that most gas-phase clusters will have three-dimensional globularlike (possibly nearly spherical) structures rather than linear or planar structures. Thus it is reasonable to assume that any moment due to orbital angular momentum can be neglected except possibly for the smallest clusters in low rotational states.

With this in mind, the dimer magnetic moment is given[12(b)] as

$$\bar{\mu}_H = \frac{\Lambda^2 M_J \mu_0}{J(J+1)} + 2M_S\mu_0 , \tag{4}$$

where J is the rotational quantum number. Since the dimer is predicted[7,13,14] to have a $^7\Delta$ ground electronic state, $\Lambda=2$, $M_S=3$, and setting $M_J \approx J$, we have

$$\bar{\mu}_H = \frac{4}{J+1}\mu_0 + 6\mu_0 . \tag{5}$$

Putting $\mu_H = 6.5\mu_0$, our experimentally measured number in Eq. (5), we find $J_{\max}=7$. Assuming the rigid rotor approximation,

$$J_{\max} = 0.5896(T_R/B)^{1/2} - \tfrac{1}{2} , \tag{6}$$

where $J_{\max}$ is the most highly populated rotational state. For Fe_2 with a rotational constant[15] ~ 0.16 cm^{-1}, and $J_{\max}=7$, the rotational temperature is calculated to be $T_R = 24$ K, quite consistent with our experimental estimates of T_R deduced from measurements of the time-of-arrival profiles. Note also that the moment due to orbital angular momentum, the first term in Eq. (4), is considerably smaller than the moment due to spin, even for the dimer. The first term will be even smaller for larger clusters, since the moment of inertia increases with cluster size.

The trimer, for instance, which is predicted[7] to have $S=4$ and have an equilateral triangular structure with a metal-metal bond length of ~ 2 Å, will be expected to have a spin magnetic moment of $8\mu_0$. This compares very favorably to our experimentally measured value of $8.1\mu_0$.

The magnetic moment of iron dimer monoxide is identical to that of the dimer within our experimental uncertainties. We are not aware of theoretical estimates for the spin of this "cluster," but the fact that the dimer oxide and dimer moments are the same suggests that the molecular binding of an oxygen atom to an iron dimer does not greatly perturb the spin character of the dimer. This in turn suggests that the dimer spin character is predominantly determined by the metal d electrons.

A. Model for depletion

Next we present a simple quantitative model which will allow us to use data such as those shown in Fig. 7, and Table III, to put bounds on the magnetic moments of larger clusters. All iron clusters contain an even number of electrons, i.e., have integer S, and therefore a nonmagnetic $M_S=0$ substate exists for each cluster. We continue to assume that under high-field conditions the coupling between spin and orbital or rotational angular momentum is weak compared to the spin coupling to the magnetic field, and the spin is spatially quantized along the magnetic field direction with $2S+1$ values of M_S. Contributions to the magnetic moment from orbital angular momentum will be negligible except possibly for very low rotational states which will be sparsely populated.

With this picture in mind, the maximum on-axis depletion factor is given by $I_0/(2S+1)$, where I_0 is the on-axis ion signal at zero-field gradient. This maximum depletion is not obtained in practice because of the limited deflecting power of the magnet and the finite spatial width of the molecular beam. From Fig. 5 the ratio of the zero gradient to the maximum gradient signal shows that on-axis depletion of the iron atom ($J=4$ in the ground state) is less than that predicted. At the highest fields I_0 is reduced by a factor of ~ 6 compared to the expected value of 9. For all clusters the on-axis signal is reduced by a factor of ~ 4 at the largest magnetic field gradient as shown in Table III.

From spatial scans such as those shown in Figs. 3 and 4, we calculate that a cluster must possess a minimum magnetic moment which is greater than or equal to $0.64\, n\mu_0$ in order to be deflected out of the detection region[16] defined by the overlap of the ionizing laser beam and the molecular beam. n is the number of atoms in the cluster. As an example, this means that the $M_S=0$ as well as the $M_S=\pm 1$ and ± 2 substates of Fe_9 will not be completely deflected out of the detection zone. For Fe_9, as well as all other clusters, depletion factors between 3 and 5 are measured. The maximum depletion factor for Fe_9 could be as high as 21—27.[17] With five of 21 substates not expected to be deflected out of the detection region experimental depletion factors of ~ 4 are understandable.

To become more quantitative, we now consider how the variation of the spin per atom as a function of cluster size will be reflected in depletion measurements for three cases: (i) The magnetic moment per atom decreases with size. (ii) The magnetic moment per atom remains constant with cluster size. (iii) The magnetic moment per atom increases with cluster size.

In case (i) the depletion factor will decrease with increasing cluster size since deflection will decrease with decreasing moment per atom, i.e., $d \propto \mu/m$ [Eq. (1)]. Although total depletion factors are smaller than expected for ground-state clusters, they do not decrease with increasing cluster size. Case (i) is not consistent with the experimental observations.

In case (ii) the depletion factor will remain constant (or possibly decrease slowly) with increasing cluster size. The deflection of the highest M_S magnetic substate will remain constant, but the total number of substates increase linearly with S. The finite deflecting power of the magnet eventually will result in some of the lowest M_S magnetic substates not being deflected out of the detection zone. The net result will be that the depletion factor will begin to decrease with increasing cluster size for sufficiently large clusters.

Case (iii) predicts that the depletion factor will increase, remain nearly constant, or eventually even decrease for

sufficiently large clusters, depending upon the actual value of the increase in moment per atom relative to the spatial extent of the clusters.

Only in cases (ii) and (iii) is a nearly constant depletion to be expected. This suggests the very exciting result that the moment per atom for iron clusters does not decrease, but at least remains constant, or possibly even increases with increasing cluster size. The above model explains why the measured on-axis depletion factors for all clusters are smaller than expected, and in addition why they fall into a narrow range of values centered around 4 with no obvious overall trend toward higher or lower values with increasing cluster size.

To demonstrate the quantitative validity of this model, we use a Gaussian fit to the experimental beam profile measured at zero gradient, and perform model calculations to predict the spatial profile expected from the sum of $2S+1$ magnetic substates, each undergoing a deflection given by Eq. (1) and each having the initial beam shape but only $2S+1$ of the initial intensity. The calculated depletion factor is simply that given by the ratio of the signal for the undeflected beam to that of the deflected beam. The spatial width, over which both profiles are integrated to give their respective signals, is set by the spatial width of the ionizing laser beam. S is then adjusted to give the best fit to the data.

As a first example, we assume the magnetic moment is that of the bulk, $2.2\mu_0$ per atom, or $\sim 20\mu_0$ for Fe_9 and $33\mu_0$ for Fe_{15}. The calculated depletion factors are 4.2 and 4.0 for Fe_9 and Fe_{15}, respectively, below the experimental values of 4.8 (see Table III). Using the theoretical values of $26\mu_0$ and $40\mu_0$ for Fe_9 and Fe_{15}, depletion factors of 5.4 and 5.0 are calculated; these are somewhat higher than the experimental values. For Fe_3 our model calculations predict a slightly smaller magnetic moment than that predicted assuming the bulk value of $2.2\mu_0$ per atom. However, as shown earlier, the trimer magnetic moment determined from magnetic field scans (Fig. 6) is $2.7\mu_0$ per atom.

In addition to the effect of finite spatial resolution, which has been shown to substantially reduce on-axis depletion, other effects which might influence the measured depletion factors include population of lower spin electronic states, spin changing transitions in the magnet, and dissociative ionization. For instance, significant population of electronic states other than the ground electronic state would reduce depletion if these are of lower spin. For the atom the measured depletion is about 6, and not the factor of 9 expected if only the $^5D_4$ state is populated. The iron atom has several low-lying electronic states, $^5D_3$, $^5D_2$, $^5D_1$, and $^5D_0$. If the electronic "temperature" was on the order of 1000 K, we would predict a depletion factor of ~ 4 and not 9. At 300 K the depletion factor would be predicted to be 8.3. A depletion factor of ~ 6 for the atom can be explained by invoking a Boltzmann distribution of excited electronic states at a temperature of ~ 700 K. Similar effects may be active in the clusters, leading to reduced depletion factors. If so, our depletion model will tend to *underestimate* depletion factors and thus the moments of the larger clusters.

A spin flip during passage of the cluster through the magnet would lead to less deflection and reduce depletion. However, a spin flip is most probable at either the entrance or exit to the magnet where the field changes most rapidly. Spin flips at the entrance or exit of a single magnet as used in these experiments would not alter the magnetic deflection pattern to any measurable extent and will be unimportant in the interpretation of these experiments.

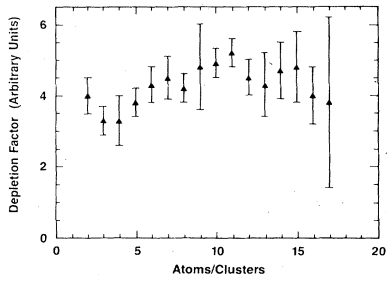

FIG. 8. Depletion factor as a function of cluster size. These data are obtained for on-axis depletion as exemplified by Fig. 7.

Lastly, we note that laser-induced dissociative ionization will produce daughter cluster ions from parent clusters. The ion signal at a particular mass would then consist of contributions from both the indigenous concentration of the small clusters as well as that from fragmentation of larger clusters.

Although fragmentation effects may not be completely absent, they are minimized by reducing the ionizing laser intensity to levels at which the ion signals only vary linearly with intensity for factors of 4 increase or decrease in intensity, and no appreciable change in the shape of the singly ionized cluster mass spectrum is detected. We note that at 2 to 3 orders of magnitude higher laser intensity, severe fragmentation is instantly obvious with the nearly complete disappearance of cluster ion signals concomitant with a large increase in the Fe-atom ion signal. In any case, for an off-axis magnetic field scan, the highest moment substate will still be the first to appear as signal. Thus, when signal is adequate, it still remains the desired mode of measurement.

The overall constancy of the depletion factor as a function of cluster size for $n=2$ to $n=17$ is interpreted to mean the magnetic moment per atom is independent of cluster size, which implies that the moments increase linearly with cluster size. In a more speculative note, we see from examination of Fig. 8 that some variation of the magnetic moment per atom occurs as well as an overall trend toward slightly higher moments per atom (i.e., higher depletion) with increasing cluster size. We are presently redesigning our apparatus to increase the spatial resolution and signal to noise in order to make more precise measurements of the magnetic moments using both off-axis magnetic field scans and on-axis depletion measurements.

B. Comparison with theory

These findings are also consistent with self-consistent-field $X\alpha$ scattered-wave (SCF-$X\alpha$-SW) theoretical predic-

tions concerning the magnetic behavior of iron clusters, in which the stability of the high spin-polarized structures relative to the nonmagnetic state for iron clusters are explained as the tendency of the high spin system to maximize d bonding.[6,7] For iron clusters of 4, 9, and 15 atoms, the total spin magnetic moments are calculated[6(a)] to be $12\mu_0$, $24\mu_0$, and $40\mu_0$, respectively, with spin per atom of 3, 2.67, and 2.67, respectively. Calculations using spin density functional theory[8] in the local approximation obtain somewhat higher values of $26\mu_0$ and $44\mu_0$ for the magnetic moments of Fe_9 and Fe_{15}, respectively, but still in reasonable agreement with earlier calculations.

Recent geometry-optimized spin-polarized SCF-$X\alpha$-SW molecular-orbital calculations[7] for the iron dimer and $8\mu_0$ for the trimer, i.e., spin per atom of 3 and 2.67, respectively. Experimentally we find that the iron dimer and trimer have magnetic moments $(6.5\pm1)\mu_0$ and $(8.1\pm1)\mu_0$, respectively.

As shown above, our measurements suggest that small iron clusters have magnetic moments $\geq 2.2\mu_0$/atom,[9] that of bulk iron, which are consistent with theoretical predictions[6-8] of $2.7\mu_0$/atom to $3\mu_0$/atom for clusters ranging in size from 2 to 15 atoms. Two different theoretical calculations have predicted that the surface magnetism for ferromagnetic iron is enhanced relative to the bulk, and in fact is different for the Fe(100) and the Fe(110) surfaces of pure bcc iron. In particular, spin polarizations of 2.90 and 2.98 electrons per atom are found for the Fe(100) surface[18,19] and 2.55 for the Fe(110) surface,[18] either of which is quite consistent with our experimental values on these small clusters. Possibly this is not completely fortuitous, since small clusters must of necessity have more surfacelike atoms than bulklike atoms. In contrast, one report[20] on the magnetic properties of Fe microclusters (distribution of cluster sizes unknown) embedded in a zeolite matrix has suggested that smaller clusters ($\sim$7 atoms in size) exhibit *reduced* magnetic moments ($1.1\mu_0$/atom), considerably below both our gas-phase values and theoretical predictions. However, as the authors point out, their observed decrease in the magnetization may be due to charge transfer from the cluster to the zeolite matrix, effectively reducing the magnetic character of the sample.

The enhanced paramagnetism exhibited by the iron oxide clusters could result from a physical expansion of the cluster upon incorporation of oxygen into the cluster with the subsequent increase of the average metal-metal bond lengths. This would manifest itself as more localized d electron density about the individual metal atoms of the cluster. The spin polarization and magnetization increase could thus be rationalized for oxide containing clusters. This picture is consistent with solid-state calculations,[21] where the magnetization is found to be a sensitive function of the lattice spacing. As the lattice spacing is decreased (increased) the width of the d bands for the spin-up and spin-down manifolds broaden (narrow) and overlap more (less), thus reducing (increasing) the magnetization. The magnetic character of d electron metals has been explained on the basis of the breadth and overlap of the d bands between the spin-up and spin-down electron manifolds at the equilibrium lattice spacing. Production of oxide clusters under well-controlled conditions has been demonstrated.[22] Thus quantitative magnetic measurements of other metal-oxide (as well as sulfide, hydride, 1 carbide, etc.) clusters are feasible. It will be of interest to compare the magnetic properties of these species with those of oxided species discussed earlier, which presumably are produced during the cluster growth phase, and for which the oxygen may be incorporated differently into the cluster.

V. SUMMARY

These first measurements on the magnetic properties of gas-phase iron clusters show that all bare (up to 17 atoms) and oxided (up to 7 atoms) clusters are paramagnetic. Their magnetic moments are found to increase linearly with cluster size, resulting in a constant spin per atom of $\geq 2.2\mu_0$, that of bulk iron, suggesting that these clusters are precursors to bulk ferromagnetic iron.

These experimental results confirm theoretical predictions regarding the high spin character of small iron clusters, and are consistent with a simple physical picture in which very strong spin ordering and large exchange splittings govern the electronic structure, which in turn may be regarded as relatively uncoupled from internuclear motion. In addition, it may be noted that the predicted cluster magnetic moments were regarded as sensitive to cluster geometry,[23] so that these results for paramagnetic iron clusters seem to be reassuringly consistent with well-behaved cluster growth characterized by rigid structures at low temperatures.[24] In light of the expected consequences of melting on electronic and magnetic ordering, the results are consistent with production of relatively cold clusters (10—30 K) by the supersonic jet condensation synthetic method, in answer to questions raised by Schumacher *et al.*[25] In fact, a sharp reduction in the magnetic moment with increasing temperature might provide clues on the melting of transition-metal clusters.[26,27]

ACKNOWLEDGMENTS

The authors are indebted to Professor Dudley Herschbach for useful discussions and for providing the inhomogeneous-field magnet used in these experiments. We particularly thank Professor Keith Johnson for many stimulating discussions and Ken Reichmann for his invaluable technical assistance during the course of these experiments. We also thank Professor J. Callaway for copies of reports on his work prior to publication.

*Permanent address: Department of Chemistry, University of California, Los Angeles, CA 90024.

†Present address: Los Alamos National Laboratory, Los Alamos, NM 87545.

[1]P. R. R. Langridge-Smith, M. D. Morse, G. P. Hansen, R. E. Smalley, and A. J. Merer, J. Chem. Phys. **80**, 593 (1984); D. L. Michalopoulos, M. E. Geusic, S. G. Hansen, D. E. Powers, and R. E. Smalley, J. Phys. Chem. **86**, 3914 (1982); J. B. Hopkins, P. R. R. Langridge-Smith, M. D. Morse, and R. E. Smalley, J. Chem. Phys. **78**, 1627 (1983); D. E. Powers, S. G. Hansen, M. E. Geusic, D. L. Michalopoulos, and R. E. Smalley, *ibid.* **78**, 2866 (1983); M. D. Morse, J. B. Hopkins, P. R. R. Langridge-Smith, and R. E. Smalley, *ibid.* **79**, 5316 (1983); D. E. Powers, S. G. Hansen, M. E. Geusic, A. C. Pulu, J. B. Hopkins, T. G. Dietz, M. A. Duncan, P. R. R. Langridge-Smith, and R. E. Smalley, J. Phys. Chem. **86**, 2556 (1982); M. D. Morse, G. P. Hansen, P. R. R. Langridge-Smith, Lan-Sun Zheng, M. E. Geusic, D. L. Michalopoulos, and R. E. Smalley, J. Chem. Phys. **80**, 5400 (1984).

[2] V. E. Bondybey and J. H. English, Chem. Phys. Lett. **94**, 443 (1983); J. Chem. Phys. **79**, 4746 (1983); V. E. Bondybey, G. P. Schwartz, and J. H. English, *ibid.* **78**, 11 (1983); G. P. Schwartz, V. E. Bondybey, J. H. English, and G. J. Gualtieri, Appl. Phys. Lett. **42**, 952 (1983).

[3]N. F. Ramsey, *Molecular Beams* (Oxford University Press, London, 1956).

[4]W. D. Knight, R. Monot, E. R. Dietz, and A. R. George, Phys. Rev. Lett. **40**, 1324 (1978).

[5]E. A. Rohlfing, D. M. Cox, and A. Kaldor, Chem. Phys. Lett. **99**, 161 (1983); J. Phys. Chem. **88**, 4497 (1984); J. Chem. Phys. **81**, 3322 (1984); E. A. Rohlfing, D. M. Cox, R. Petkovic-Luton, and A. Kaldor, J. Phys. Chem. **88**, 6227 (1984).

[6]C. Y. Yang, K. H. Johnson, D. R. Salahub, J. Kaspar, and R. P. Messmer, Phys. Rev. B **24**, 5673 (1981); D. R. Salahub and R. K. Messmer, Surf. Sci. **106**, 15 (1981).

[7]E. A. Rohlfing, D. M. Cox, A. Kaldor, and K. H. Johnson, J. Chem. Phys. **81**, 3846 (1984).

[8]K. Lee, J. Callaway, and S. Dhar, Phys. Rev. B **30**, 1724 (1984); K. Lee, J. Callaway, K. Kwong, R. Tang, and A. Ziegler, *ibid.* **31**, 1796 (1985).

[9]H. Danan, A. Herr, and A. J. P. Meyer, J. Appl. Phys. **39**, 669 (1968).

[10]M. A. D. Fluendy, R. M. Marton, E. E. Muschlitz, and D. Herschbach, J. Chem. Phys. **46**, 2172 (1967); R. R. Herm and D. Herschbach, UCRL Report No. 10526, University of California Radiation Laboratory, Berkeley, Calif., Oct. 1962 (unpublished).

[11]J. P. Toennies and K. Winkelmann, J. Chem. Phys. **66**, 3965 (1977).

[12]G. Herzberg, *Electronic Spectra of Polyatomic Molecules* (Van Nostrand/Reinhold, New York, 1966); G. Herzberg, *Spectra of Diatomic Molecules,* 2nd ed. (Van Nostrand/Reinhold, New York, 1950).

[13]D. Guenzburger and E. M. B. Saitovitch, Phys. Rev. **24**, 2368 (1981).

[14]H. M. Nagarathna, P. A. Montano, and V. M. Naik, J. Am. Chem. Soc. **105**, 2938 (1983).

[15]The dimer bond length of ~ 2 Å was reported by (a) P. A. Montano and G. K. Shenoy, Solid State Commun. **35**, 53 (1980); (b) H. Purdum, P. A. Montano, G. K. Shenoy, and T. Morrison, Phys. Rev. B **25**, 4412 (1982).

[16]For example, if it is assumed that two magnetic substates are spatially resolved when the signal intensity drops by 50% between the peaks of two adjacent ($\Delta M_S = 1$) substates, then the minimum magnetic moment which is required for such a deflection can be determined from Eq. (1). The molecular beam profile shown in Fig. 4 is closely approximated by a Gaussian. For a Gaussian beam shape this resolution is obtained for a separation of 1.414 FWHM. The FWHM of the iron atom peak is 0.64 mm. Thus for states to be resolved the minimum deflection per iron atom is 0.89 mm. From Fig. 4 the deflection of the $M_s = 1$ substate of the atom (magnetic moment $1.5\mu_0$) is separated from $M_s = 0$ by 1.26 mm for a magnetic field gradient of 50.8 kG/cm. At 84 kG/cm gradient used in obtaining Fig. 7 the minimum moment which can be resolved is $0.64\mu_0 n$, where n is the number of atoms in the cluster.

[17]If we assume the magnetic moment per atom is given by the bulk value of $2.2\mu_0$ per atom, a total moment of $\sim 20\mu_0$ is expected for Fe_9. This implies 20 unpaired electrons with $2S+1=21$. Theoretical calculations for Fe_9 predict 26 unpaired electrons yielding $2S+1=27$.

[18]R. H. Victora, L. M. Falicov, and S. Ishida, Phys. Rev. B **30**, 3896 (1984).

[19]S. Ohnishi, A. J. Freeman, and M. Weinert, Phys. Rev. B **28**, 6741 (1983).

[20]F. Schmidt, U. Stapel, and H. Walther, Ber. Bunsenges. Phys. Chem. **88**, 310 (1984).

[21]J. C. Slater, *The Self Consistent Field for Molecules and Solids: Quantum Theory of Molecules and Solids, Vol. IV* (McGraw-Hill, New York, 1974).

[22]R. L. Whetten, D. M. Cox, D. J. Trevor, and A. Kaldor, J. Phys. Chem. **89**, 566 (1985); Phys. Rev. Lett. **54**, 1491 (1985).

[23]A. Pellegatti, B. N. McMaster, and D. R. Salahub, Chem. Phys. **75**, 83 (1983).

[24]In support of this claim are measurements of the strong temperature dependence of the magnetization of surface supported clusters nearing and even below the bulk Curie temperature: T. S. Cale, J. T. Richardson, and J. Ginestra, Appl. Phys. Lett. **42**, 744 (1983).

[25]E. Schumacher, M. Kappes, K. Marti, P. Radi, M. Schar, and B. Schmidhalter Ber. Bunsenges. Phys. Chem. **88**, 220 (1984).

[26]Ph. Buffat and J.-P. Borel, Phys. Rev. A **13**, 2287 (1976).

[27]R. S. Berry, J. Jellinek, and G. Natanson, Phys. Rev. A **30**, 919 (1984); G. Natanson, F. Amar, and R. S. Berry, J. Chem. Phys. **78**, 399 (1983).